SPATIAL CORRELATION OF VELOCITY AND HEAT TRANSFER DOWNSTREAM OF A BACKWARD FACING STEP USING 2D-3C PIV AND IR THERMOGRAPHY

Shunsuke Yamada
Department of Mechanical Engineering
National Defense Academy
Hashirimizu, 1-10-20, Yokosuka, Kanagawa, 239-8686, Japan
yamadas@nda.ac.jp

Hajime Nakamura
Department of Mechanical Engineering
National Defense Academy
Hashirimizu, 1-10-20, Yokosuka, Kanagawa, 239-8686, Japan
nhajime@nda.ac.jp

ABSTRACT

In the present study, the correlative relation between the heat transfer and the flow behaviors in the near-wall region downstream of a backward facing step is presented. The instantaneous flow and convective heat transfer distributions are measured using two-dimension-three component (2D-3C) PIV system and a high-speed infrared thermography at the same time. Using this system, the unsteady flow behavior in the xz cross section and the heat transfer on the heated wall are investigated for the Reynolds number range of from 2.5×10^3 to 7.6×10^3. In order to discuss the correspondence of the near-wall flow and the heat transfer, the cross correlation coefficient of these distributions is calculated, and the forward and downwash flows appear to enhance the heat transfer in the near-wall region.

INTRODUCTION

Recently, the suppression of CO_2 emissions due to global warming and the effective utilization of energy resources such as fossil fuels and natural gas have become important problems. At present, the thermal engine, which is widely used, transduces thermal energy into power and electric energy through the working fluid. The design of a thermal engine having a high driving efficiency requires consideration of three-dimensional and unsteady characteristics because the working fluid in this engine exhibits a turbulent flow.

In a turbulent channel flow, the turbulent Prandtl number, Pr_τ, plays a crucial role in modelling turbulent transport. In a previous study, the turbulent Prandtl number ranged from 0.7 to 0.9 based on the numerical data for a channel flow, and the dissimilarity between the heat-flux and flow fluctuations, which are related to the momentum and thermal transport, was discussed (Kawamura, et al., 1999). In the separated and reattached flow, the heat transfer coefficient increases around the reattachment region. In order to understand this

phenomenon, many researchers have investigated the aspects of fluid and thermal dynamics (Seaban, 1964, Vogel et al. 1985). However, few experimental studies have investigated the similarity or dissimilarity between the momentum and scalar transport in the separated and reattached flow. In order to understand the similarity or dissimilarity in the separated flow, we suggest the simultaneous measurement of the flow and the thermal field using 2D-3C PIV and a high-speed infrared thermography combined system. The correlation of each velocity in the xz cross section and heat transfer fluctuations on the heated wall are investigated behind a backward facing step for a Re_H range of from 2.5×10^3 to 7.6×10^3.

EXPERIMENTAL SETUP AND METHOD
Wind tunnel and co-ordinate system

The experiments were carried out in an open-type wind tunnel having a rectangular cross section of 400 mm in height and 150 mm in width, as shown in Fig. 1(a). The working fluid was air. A flat plate (aluminium plate) of 1200 mm in length was placed horizontally at mid-height in the wind tunnel. The step height, H, was 19 mm. A measurement surface, which was heated for heat transfer measurement, was positioned behind the step edge. Turbulent flow was induced by a trip wire of 2 mm in diameter, which was mounted 870 mm upstream of the step edge. The origin of the coordinate system used in the present study was located mid-span of the bottom wall of the step edge. In this coordinate system, x denotes the streamwise direction, y denotes the transverse direction, and z denotes the spanwise direction. The streamwise turbulent intensity of the mainstream was approximately 0.5%. The main stream velocity, u_0, ranged from approximately 2 to 6 m/s. The Reynolds number, Re_H, based on the step height and the mainstream velocity upstream of the step edge ranged from approximately 2.5×10^3 to 7.6×10^3.

Fig. 1(b) shows a schematic diagram of the heated plate. The heated plate was fabricated from acrylic resin and had three sections removed. These sections were covered with thin titanium foil sheets (61 mm in length, 100 mm in width, and 2.1 μm in thickness) arranged in the streamwise direction. In the heated plate, air layers 1 mm in thickness exist between the heated titanium foil and the aluminium plate (see Fig. 1(b)). Since the titanium foil and the aluminium plate were heated to approximately the same temperature, the heat conduction loss inside the test plate was suppressed. The temperature inside the heated aluminium plate was measured by thermocouples (TC) at $x = 62$ and 124 mm. Both sides of these thin foils were tightly adhered to electrodes with a high-conductivity bond in order to suppress contact resistance. The three sheets of these foils were heated by direct current so that the temperature difference between the surface of this foil and the mainstream flow was approximately 20 °C. The titanium foil sheets were stretched in response to tension, because the thermal expansion coefficient of the heated acrylic resin is greater than that of the titanium foil. The rms value of the vertical displacement of the thin foil using a laser displacement meter was approximately 2 μm. The surface of the thin foil was measured using a high-speed infrared thermograph, so that high-speed thermal fluctuation was observed due to the low heat capacity of the thin titanium foil.

Experimental apparatus of 2D-3C PIV and IRT
Figure 1(c) shows a schematic diagram of the simultaneous measurement system. The PIV camera shutter and the emission of a double-pulse laser were synchronized by function generator 1. In Fig. 1(c), two cameras (Motion Scope M3, IDT) and a double-pulse laser (Solo-PIV II-20, New Wave Research) were used to measure the flow fluctuation in the xz cross section in the x/H range of 3.2 to 6.3 (see Fig. 1(d)). The laser light sheet was located at $y/H = 0.06$ and 0.10. The camera frame rate for PIV measurement was 15 frames per second (fps). The thermal fluctuation was observed by a high-speed infrared thermograph (SC4000, FLIR, IRT) at 300 fps. A schematic diagram of the IRT setup is shown in Fig. 1(d). The thermal fluctuation on the surface of the heated plate was measured in the x/H range of from 3.2 to 6.3. Based on the time series of thermal distribution, the heat transfer coefficient was restored by the unsteady heat conduction equation (Nakamura and Yamada, 2013).

Inverse analysis of thermal conduction equation
The temperature on the surface of the titanium foil measured by an infrared thermal imaging camera, T_w, was obtained from the following equation:

$$E = \varepsilon\, B(T_w) \; + \; (1-\varepsilon)\, B(T_{amb}) \tag{1}$$

where E is the spectral emissive power detected by IRT, $B(T)$ is the calibration function of the IRT, and ε is the spectral emissivity of the foil for IRT The terms on the right-hand side of Eq. (1) denote the emissive power from the test surface, T_w, and the ambience, T_{amb}, respectively. In this measurement, the distance between the infrared thermal imaging camera and the test surface was approximately 400 mm, so that τ was approximately 1.0.
Fig. 2 shows a schematic diagram of the heat transfer model from the heated plate. The local and instantaneous heat transfer coefficients were obtained from the
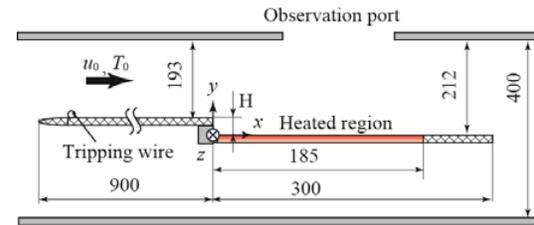
(a) Wind tunnel
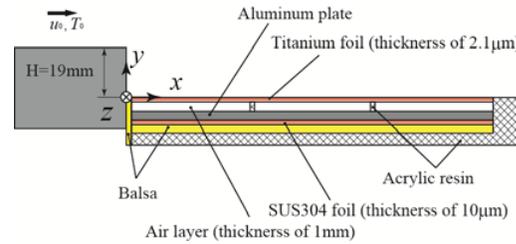
(b) Heated plate
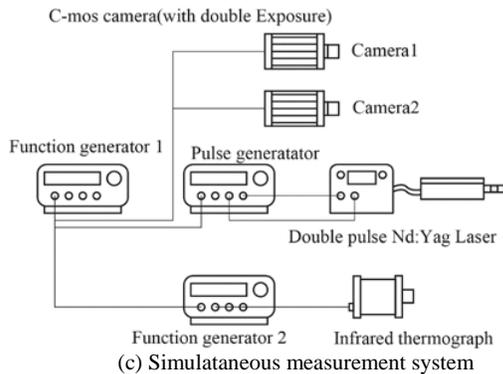
(c) Simulataneous measurement system
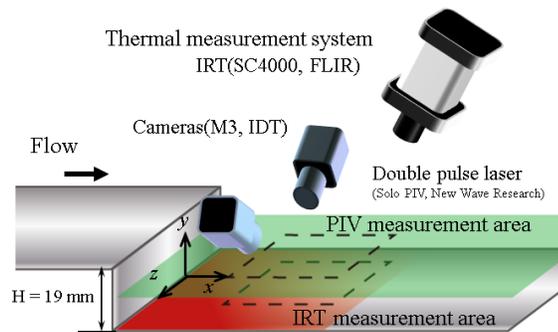
(d) Arrangement of PIV camera and IRT

Figure 1. Schematic diagram of the experimental apparatus

following equations:

$$h = \frac{\dot{q}_{in} - \dot{q}_{cd} - \dot{q}_{rd} - \dot{q}_{rdi} + A - B}{T_W - T_0} \qquad (2)$$

where

$$A = \lambda_t \left(\frac{\partial^2 T_W}{\partial x^2} + \frac{\partial^2 T_W}{\partial z^2} \right) \qquad (3)$$

and

$$B = c_t \rho_t \delta_t \frac{\partial T_W}{\partial t} \qquad (4)$$

where $\dot{q}_{in}$ is the input heat flux to the foils due to the Joule heating, $\dot{q}_{cd}$ is the heat flux from the foil due to the conduction and $\dot{q}_{ra}$ and $\dot{q}_{rai}$ are the radiation heat fluxes away from and into the heated plate, respectively. The inverse heat conduction equation, given by Eq. (2), includes both lateral heat conduction though the foil given by Eq. (3) and the temporal delay due to the heat capacity of the foil given by Eq. (4). The heat conduction to the air layer inside the heated plate was calculated based on the temperature distribution inside the air layer (thickness $\delta_a = 1$ mm), which can be determined by solving the following heat conduction equation:

$$\dot{q}_{cd} = -\lambda_a \left(\frac{\partial T_a}{\partial y} \right)_{y=0} \qquad (5)$$

and

$$c_a \rho_a \frac{\partial T_a}{\partial t} = \lambda_a \left(\frac{\partial^2 T_a}{\partial x^2} + \frac{\partial^2 T_a}{\partial y^2} + \frac{\partial^2 T_a}{\partial z^2} \right) \qquad (6)$$

Since the temperature of the aluminium plate inside the heated plate was assumed to be steady and uniform, the boundary condition given by Eq. (6) on the aluminium plate side can be assumed to be the mean temperature of the aluminium plate as measured using the calibrated thermocouples. The temperature of the air layer inside the heated plate in Eq. (6) was calculated using the alternative direction implicit (ADI) method with respect to the x and z directions.

The finite difference method was used to calculate the heat transfer coefficient, h, using Eq. (2). The spatial derivative terms of A were calculated using the second-order central difference with the pixel spacing ($\Delta x \approx \Delta z \approx 0.53$ mm). Moreover, the temporal derivative term of B was calculated using the central difference with the time step of a frame interval ($\Delta t = 1/300$ second).

Inlet condition upstream of the step

Figures 3(a) and 3(b) show the temporal-averaged and rms values of the streamwise velocities measured by hot-wire anemometer upstream of the step edge ($x = -10$ mm). Moreover, Table 1 summarizes the boundary layer and momentum thicknesses and the wall-friction velocity and length used to define the Reynolds number, respectively. Each quantity in these figures was nondimensionalized by friction velocity, which was estimated by fitting an eddy-viscosity-based profile to the mean velocity profile near the wall. In Fig. 3(a), the measurement accuracy of the streamwise velocity is insufficient near the wall at a y^+ of approximately 2, but the profiles in the present study are coincident with the results of DNS in the log-law region
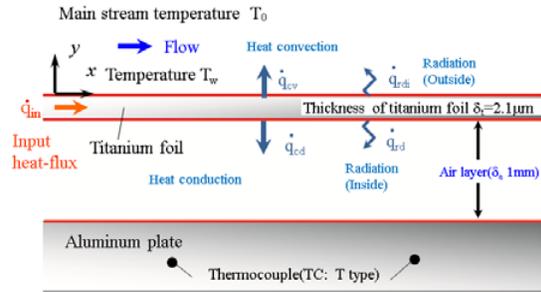
Figure 2. Schmetic of the heat transfer from the heated plate
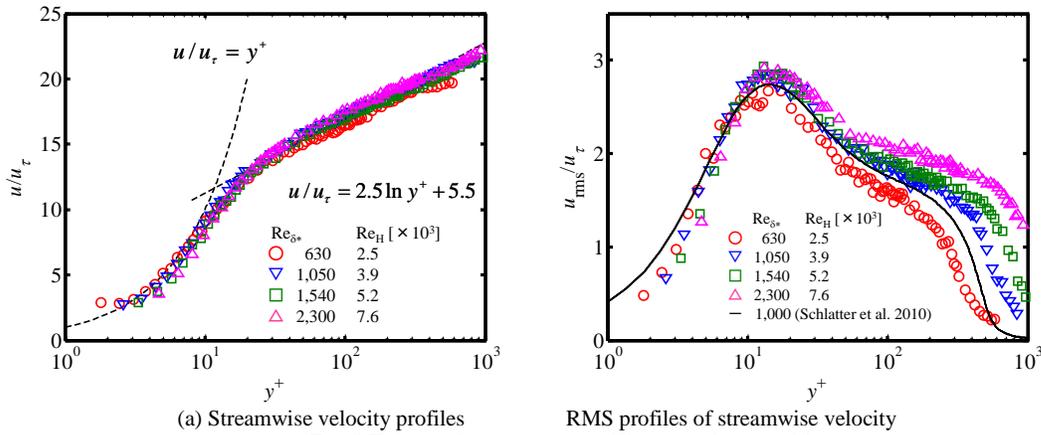
(a) Streamwise velocity profiles   RMS profiles of streamwise velocity
Fig. 3 Flow condition upstream of the step edge($x = -10$ mm).

3

from the viscous sublayer to the logarithmic layer. The maximum rms value appears at a y^+ of 15, and the peak position obtained in the present study and the DNS (Schlatter and Örlü, 2010) at a $Re_{\delta*}$ of approximately 1,000 are approximately the same, as shown in Fig. 3(b). However, the difference between the results of the present study and the previously reported numerical results is large in the log-law region, because the experimental conditions of the turbulent enhancement by the trip wire, the turbulent intensity in the mainstream, and the aspect ratio of the cross section normal to the streamwise direction in the wind tunnel are different from the numerical results.

EXPERIMENTAL RESULTS AND DISCUSSIONS
Instantaneous velocity and heat transfer profiles

Figures 4 and 5 show the instantaneous contour distribution of (a) streamwise velocity, (b) transverse velocity, and (c) heat transfer coefficient at $y/H = 0.10$ and 0.06, respectively, in the xz cross section at $Re_H = 2.5\times10^3$. Moreover, the vectors of the streamwise and spanwise velocity components are shown in (a) and (b) of these figures. As shown in Fig. 4(a), the streamwise velocity increases downstream of $x/H = 5.0$, and the distribution of the region of increasing streamwise velocity is not uniform in the spanwise direction. The reattachment point appears to exist in the x/H range of from 4.5 to 5.0. The local maximum and minimum of the transverse velocity distributions are observed in Fig. 4(b). However, in the

Table 1 Flow parameters upstream of the step edge ($x = -10$ mm)

$Re_H [\times10^3]$	$Re_\delta [\times10^3]$	Re_θ	δ_{99} [mm]	θ [mm]	u_τ [m/s]	l_τ [mm]
2.5	6.5	630	0.049	0.0483	0.100	0.153
3.9	11.5	1050	0.059	0.00537	0.144	0.107
5.2	18.0	1540	0.069	0.0589	0.186	0.082
7.6	27.3	2300	0.070	0.0586	0.261	0.059
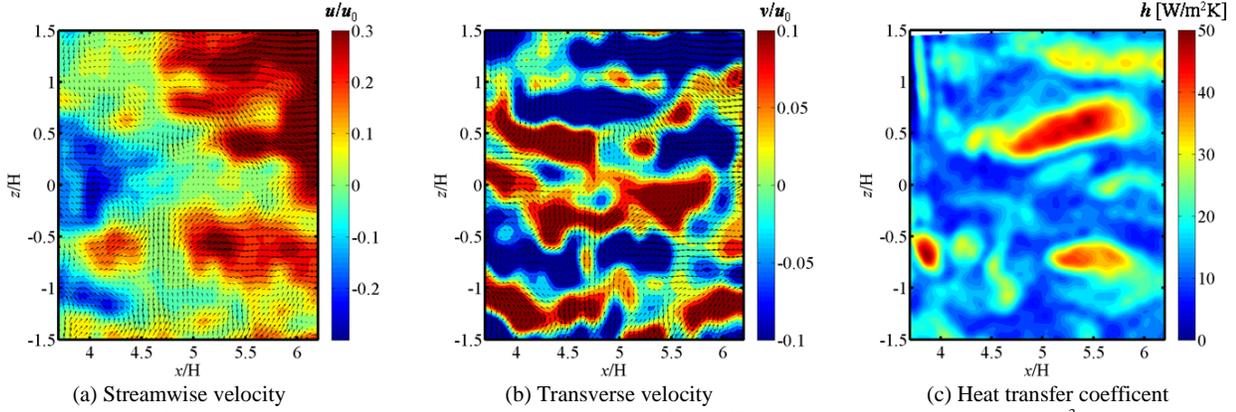
(a) Streamwise velocity (b) Transverse velocity (c) Heat transfer coefficent
Fig. 4 Velocity($y/H = 0.10$ in the xz plane) and heat transfer coefficient (heated plate) at $Re_H = 2.5\times10^3$.
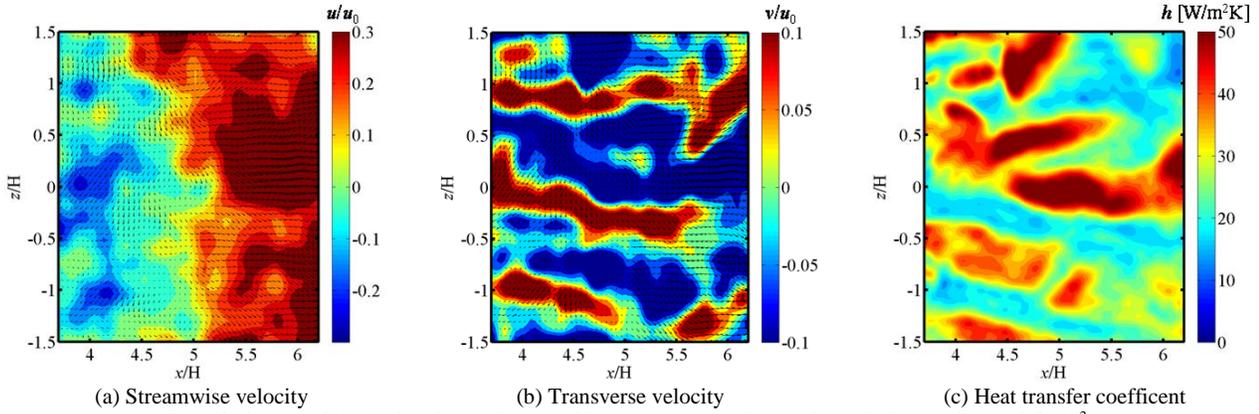
(a) Streamwise velocity (b) Transverse velocity (c) Heat transfer coefficent
Fig. 5 Velocity($y/H = 0.06$ in the xz plane) and heat transfer coefficient (heated plate) at $Re_H = 2.5\times10^3$.

4

spatial distributions of the velocity components in Figs. 4(a) and (b) and the heat transfer coefficient in Fig. 4(c), the locally maximum and minimum regions of heat transfer coefficient, h, are not qualitatively consistent with those of the velocity components at $y/H = 0.10$. As shown in Fig. 5(a), the reverse and forward flows appear upstream and downstream of $x/H = 5.0$ at $y/H = 0.06$. Fig. 5(b) shows the transverse flow toward the positive direction (upwash flow) at $z/H = 0$ and ± 1.0, and the flow toward the negative direction (downwash flow) at $z/H = \pm 0.5$. The distributions of the upwash and downwash flows exhibit the wavy fluctuation in the spanwise direction. As shown in Fig. 5(c), the high heat transfer region at $z/H = \pm 0.5$ extends in the flow direction, and the unsteady distribution appear on the heated plate. The transverse velocity and heat transfer coefficient distributions are non-uniform in the fluid and thermal fields.

Correlative relation between flow and thermal fluctuations in the spanwise direction

In order to compare the spatial correspondence relationship between the flow and thermal behavior at the same time, Figs. 6(a) through 6(c) show the isolines of each velocity component and the contour of the heat transfer coefficient. The red and blue isolines represent the positive and negative directions, respectively, of each velocity component. Fig. 6(b) shows that the negative and positive regions of the transverse velocity distributions qualitatively correspond to the high and low regions, respectively, of the heat transfer coefficient. However, it is qualitatively difficult to confirm the correspondence between streamwise and spanwise velocity distributions and the heat transfer coefficient distribution, as shown in Figs. 6(a) and (c).

Figs. 7(a) and 7(b) show the rates of the negative and positive correlations, I_n/I_a and I_p/I_a, between the heat transfer coefficient and each velocity fluctuation in the spanwise direction in the x/H range of from 4.2 to 5.8 at $y/H = 0.06$ (I_n and I_p are the number of image when the cross correlation coefficient between the each velocity and the heat transfer coefficient is under -0.2 and over 0.2, respectively. Moreover, I_a is the number of images of flow and thermal fields that correspond in time, which is 56). The plus or minus subscripts in the horizontal axis labels of Fig. 7 indicate the rates of negative and positive correlations. The correlation between the streamwise and transverse velocities and the heat transfer represents high positive and negative values. However, the correlation between the spanwise velocity and the heat transfer is low in comparison with the streamwise and transverse velocities. Moreover, the negative and positive correlations of the spanwise velocity are both low. The fluctuation of the heat transfer in the spanwise direction corresponds to that of the forward and downwash flows in the near-wall region. In the case of a turbulent flow, Piller

(a) Streamwise velocity   (b) Transverse velocity   (c) Spanwise velocity
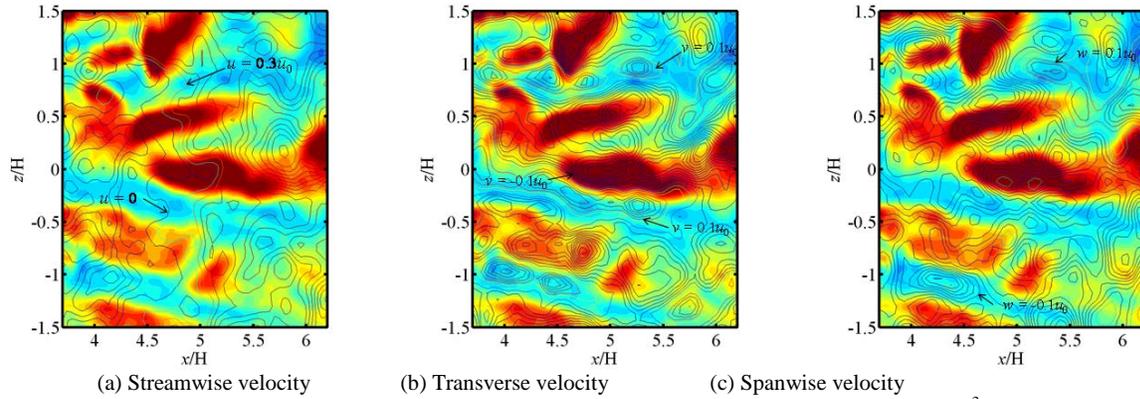
Fig. 6 Correspondence relationship between instantaneous flow and heat transfer ($Re_H = 2.5 \times 10^3$, $y/H = 0.06$).

(a) Re_H of 2.5×10^3 (b) $x/H = 5.8$ for the Re_H range of 2.5×10^3 to 7.6×10^3
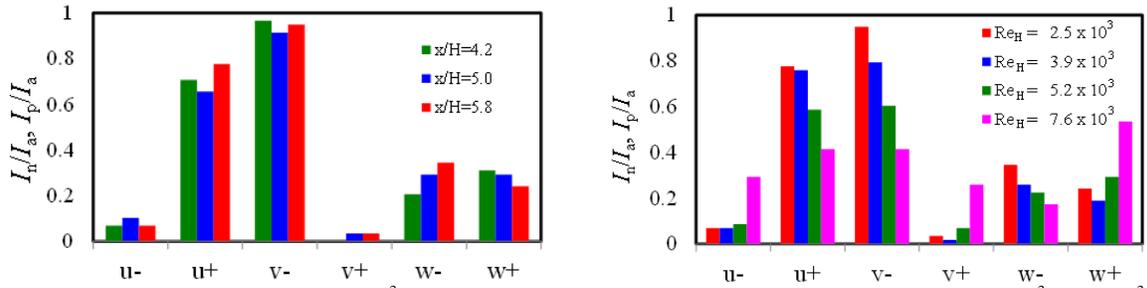
Figure 7. Rate of spatial correlation values between each velocity and heat transfer fluctuation at y/H of 0.06.

et al. (2007) and Abe et al. (2004) reported that the correlation between the fluctuation of the streamwise flow and temperature became high near the wall. Moreover, Gallo et al. (2012) reported that the impinging flow promoted by the strong vortex, enhances the convective heat transfer. The results of the present study have demonstrated a similar tendency using the combined 2D-3C PIV and IRT measurement system.

Figure 7(b) shows the rates of negative and positive correlations at x/H = 5.8 in the Re_H range of from 2.5×10^3 to 7.6×10^3. The rate of the negative and positive correlation between the transverse, and streamwise velocities and the heat transfer, u^+ and v^-, are very high downstream of the reattachment point. These positive and negative correlation rates of the spanwise velocity are approximately the same across the Re_H range from 2.5×10^3 to 5.2×10^3. However, the rate of the correlations between all velocities and the heat transfer fluctuations decrease at a Re_H of 7.6×10^3.

SUMMARY

We established a simultaneous measurement system using 2D-3C PIV and a high-speed infrared thermograph in order to investigate the velocity and heat transfer fluctuations near the wall over a backward facing step. The fluctuation of three velocity components and heat transfer coefficients were simultaneously measured near the reattachment region for the Re_H range of 2.5×10^3 to 7.6×10^3. As a result, the high heat transfer coefficient corresponded to the increase in the forward and the downwash flow in the vicinity of the heated wall. The rate of the negative and positive correlation between the transverse, and streamwise velocities and the heat transfer are very high in this measurement area.

REFERENCE

Abe, H., Kawamura, H and Matsuo, Y., 2004, "Surface heat-flux fluctuations ina turbulent channel flow up to $Re_\tau = 1020$ with Pr = 0.025, 0.71," *Int. J. Heat and Fluid Flow*, 25, pp. 404-419.

Gallo, M., Astarita, T. and Carlomagno, G. M., 2012, "Thermo-fluid-dynamic analysis of the flow in a rotating channel with a sharp "U" turn," *Exp. Fluids*, 25, DOI 10.1007/s00348-012-1283-7.

Kawamura, H., Abe, H. and Matsuo, Y., 1999, "DNS of turbulent heat transfer in channel flow with respect of Reynolds and Prandtl number effects," *Int. J. Heat and Mas Transfer*, 64, pp. 892-902.

Nakamura, H. and Yamada, S., 2013, "Quantitative evaluation of spatio-temporal heat transfer to a turbulent air flow using a heated thin-foil," *Int. J. Heat and Mas Transfer*, 64, pp. 892-902.

Piller, M., 2007, "Direct numerical simulation of turbulent forced convection in a pipe," *Int. J. Numerical Methods in Fluids*, 49, pp. 583-602.

Schlatter, P. and Örlü, R., 2010, "Assessment of direct numerical simulation data of turbulent boundary layer," *Journal of Fluid Mechanics,* 659, pp116-126.

Seaban, R. A., 1964, "Heat Transfer to the Turbulent Separated Flow of Air Downstream of a Step in the Surface of a Plate," *J. Heat Transfer, Trans. ASME*, C86, pp. 259-264.

Vogel, J. C., and Eaton, J. K., 1985, "Combined Heat Transfer and Fluid Dynamics Measurements Downstream of a Backward Facing Step," *Trans. ASME J. Heat Transfer*, Vol. 107, pp.922-929